PNAS RESEARCH ARTICLE | EARTH, ATMOSPHERIC, AND PLANETARY SCIENCES
SUSTAINABILITY SCIENCE

# Estimating future climate change impacts on human mortality and crop yields via air pollution

Lee T. Murray[a,b,1], Eric M. Leibensperger[c], Loretta J. Mickley[d], and Amos P. K. Tai[e,f,g]

Affiliations are included on p. 8.

Edited by Akkihebbal Ravishankara, Colorado State University, Fort Collins, CO; received January 4, 2024; accepted July 22, 2024

**Future climate change may bring local benefits or penalties to surface air pollution, resulting from changing temperature, precipitation, and transport patterns, as well as changes in climate-sensitive natural precursor emissions. Here, we estimate the climate penalties and benefits at the end of this century with regard to surface ozone and fine particulate matter ($PM_{2.5}$; excluding dust and smoke) using a one-way offline coupling between a general circulation model and a global 3-D chemical-transport model. We archive meteorology for the present day (2005 to 2014) and end of this century (2090 to 2099) for seven future scenarios developed for Phase 6 of the Coupled Model Intercomparison Project. The model isolates the impact of forecasted anthropogenic precursor emission changes versus that of climate-only driven changes on surface ozone and $PM_{2.5}$ for scenarios ranging from extreme mitigation to extreme warming. We then relate these changes to impacts on human mortality and crop production. We find ozone penalties over nearly all land areas with increasing warming. We find net benefits due to climate-driven changes in $PM_{2.5}$ in the Northern Extratropics, but net penalties in the Tropics and Southern Hemisphere, where most population growth is forecast for the coming century.**

climate change | air quality | global food security

## Significance

Air pollution contributes to loss of life and destroys crops. Future climate change alone may make air pollution worse or better. Here, we find that biospheric responses to increasing global mean surface air temperature will lead to surface ozone increases over almost all land surfaces, contributing to human mortality and crop losses. In contrast, future changes in fine particulate matter, another type of pollution, will decrease in some areas, which will save lives. However, in areas like the Tropics and the Southern Hemisphere, where population will grow most rapidly in the coming century, concentrations of fine particles from natural sources will increase. These impacts should be considered in cost–benefit analyses of taking action to fight climate change.

Exposure to air pollution, primarily fine particulate matter under 2.5 μm in diameter ($PM_{2.5}$) and ground-level ozone ($O_3$), is the leading cause of preventable death worldwide; one in eight lives presently ends prematurely due to exposure to unhealthy air (1, 2). Ground-level ozone also damages vegetation, and its impact on crops has significant economic costs and threatens global food security (3–5). Air pollution results from the chemical processing of unfavorable emissions during unfavorable meteorological conditions (6–8). It is generally assumed that as developing countries increase their wealth in the coming century, they will begin to implement air pollution regulations and control technologies to improve citizen health, and global anthropogenic emissions will decline. This assumption is included in the shared socioeconomic pathway (SSP) anthropogenic precursor emissions for ozone and $PM_{2.5}$ (Figs. 1 and 2) developed for the most recent international climate assessment studies for the end of the century (2090 to 2099 CE) relative to the recent past (2005 to 2014 CE), which reflect this assumption (9–11). However, anthropogenic-driven climate change over this period will also change the meteorological conditions that influence air pollution, including natural precursor emissions, which may counter any anthropogenic emission reductions. When meteorological changes alone contribute to increased air pollution, it is commonly referred to as a "climate penalty" (12). However, it is also possible for meteorological changes alone to reduce air pollution, which may be considered a "climate benefit" (8, 13).

Three primary methods have been applied to estimate climate penalties and benefits. The first looks for statistical relationships between meteorological parameters and pollution levels in the recent past and then applies these relationships to future forecasted meteorology changes (e.g., ref. 14). However, this method becomes increasingly uncertain as one extrapolates further into the future, when the underlying statistical relationships may have changed. The second uses chemistry-transport models (CTMs) driven by present-day and future meteorology archived from free-running general circulation models (GCMs) in various permutations with present-day and future emissions to estimate the contribution of emission changes versus meteorology changes (e.g., ref. 12). The third uses GCMs with online interactive tropospheric chemistry, also known as chemistry-climate models (CCMs), in which simulations with future anthropogenic precursor emissions but separate present-day or future climate forcings are compared to estimate the climate impact (e.g., ref. 15). The benefit of a CTM is that it is

Author contributions: L.T.M. designed research; L.T.M., E.M.L., and L.J.M. performed research; L.T.M. analyzed data; and L.T.M., E.M.L., L.J.M., and A.P.K.T. wrote the paper.

The authors declare no competing interest.

This article is a PNAS Direct Submission.



[1]To whom correspondence may be addressed. Email: lee.murray@rochester.edu.

This article contains supporting information online at https://www.pnas.org/lookup/suppl/doi:10.1073/pnas.2400117121/-/DCSupplemental.

Published September 16, 2024.

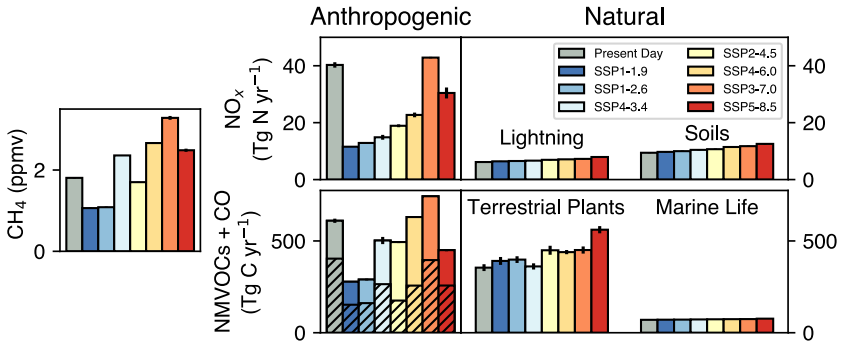


**Fig. 1.** Global prescribed anthropogenic and forecasted natural ozone precursor emissions in each simulation. The present day is 2005 to 2014 CE mean (gray). All other scenarios are 2090 to 2099 CE mean (colors). Black vertical bars show $\pm 1\sigma$ of the interannual variability for each decade. Methane ($CH_4$) is prescribed as a surface boundary condition. Diagonal hatching indicates the CO component of the nonmethane reduced carbon emissions (NMVOCs+CO).

straightforward to evaluate attribution, as its one-way coupling does not allow chemistry-climate feedbacks that can complicate the determination of cause and effect. Furthermore, CTMs do not simultaneously resolve the equations of motion and, therefore, can expend more computational resources to perform more complex chemistry than CCMs and additional scenarios. The downside to CTM studies is the severely limited availability of future forecast meteorology, which must be archived with high 4-dimensional frequency, and the simulated composition by design does not feed back onto the meteorology and, thereby, composition in the simulations.

The first exploration of climate penalties and benefits on air pollution was an analysis of future climate change on surface ozone (12). Ozone abundances were found to increase in many polluted regions but decrease across much of the rest of the world. Subsequent regional and global studies have been generally consistent with this picture, although more recent studies predict smaller penalties than the earlier studies did (13, and ref. therein). In contrast, an analysis of five free-running CCMs performed for Phase 6 of the Climate Model Intercomparison Project (CMIP6) generally found ozone climate benefits globally in a single future emission scenario. However, changes were generally insignificant over populated regions relative to the internal variability of the free-running CCMs (15). Whereas there have been numerous studies to date linking $PM_{2.5}$ pollution with meteorological variability (e.g., ref. 14), there have been far fewer explicit studies of $PM_{2.5}$ climate penalties or benefits compared to ozone. Those that have generally found a much more heterogeneous response relative to ozone, reflecting the much shorter lifetime of $PM_{2.5}$ (e.g., ref. 16).

This study utilizes a recently developed CTM framework (17, and see *Materials and Methods*) to provide a global perspective of climate change penalties and benefits on both surface ozone and $PM_{2.5}$ for multiple future climate scenarios ranging from extreme mitigation to extreme warming across the coming century. In addition, we extend the penalties and benefits beyond changes in concentration to forecasted changes in human mortality and crop production. We first describe the changes in surface air pollutants and the underlying causes in the model. We then examine the impacts on human mortality and crop losses, respectively. We end with a conclusions section.

**Forecasted Changes to Air Pollution.** Fig. 3 shows the forecasted changes in six-month seasonal maximum daily 8-h average ozone (OSMDA8) and annual-mean $PM_{2.5}$ (excluding fine mineral dust and sea-salt particles; see discussion below) at the end of the century (2090 to 2099 CE) relative to the recent past (2005 to 2014 CE) for seven future SSP scenarios. We show both the total forecasted changes and the contribution of climate change alone (*Materials and Methods*). The nomenclature for describing the SSP scenarios is "*x-y.z*," where *x* represents a socioeconomic scenario that assumes an amount of international cooperation from 1 (most) to 5 (least), and *y.z* represents the targeted end-of-century radiative forcing limit with respect to the preindustrial from 1.9 W $m^{-2}$ (extreme mitigation including carbon capture) to 8.5 W $m^{-2}$ (extreme warming; 9–11). The SSP4-3.4 scenario meets the Paris Agreement goal of limiting global mean warming to 2.0 °C above preindustrial levels, whereas only the SSP1-1.9 scenario meets the loftier goal of limiting warming to 1.5 °C. Our simulations indicate that changes in future anthropogenic precursor emissions primarily dictate the forecasted future pollution levels. However, climate change alone is forecast to cause climate penalties to surface ozone over most land locations as well as to $PM_{2.5}$ in the Tropics and Southern Hemisphere at the end of the century, but climate benefits to $PM_{2.5}$ over the Northern Extratropics. The magnitude of these penalties and benefits increases with increasing warming.

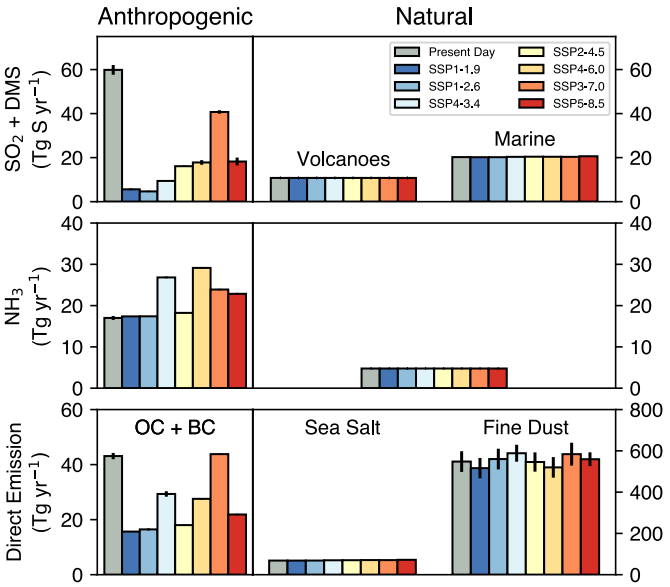


**Fig. 2.** Global prescribed anthropogenic and forecasted natural $PM_{2.5}$ precursor (rows one and two) and direct (row three) emissions in each of the simulations. NMVOC emissions shown in Fig. 1 are also $PM_{2.5}$ precursors. The present day is 2005 to 2014 CE mean (gray). All other scenarios are 2090 to 2099 CE mean (colors). Black vertical bars show $\pm 1\sigma$ of the interannual variability for each decade.

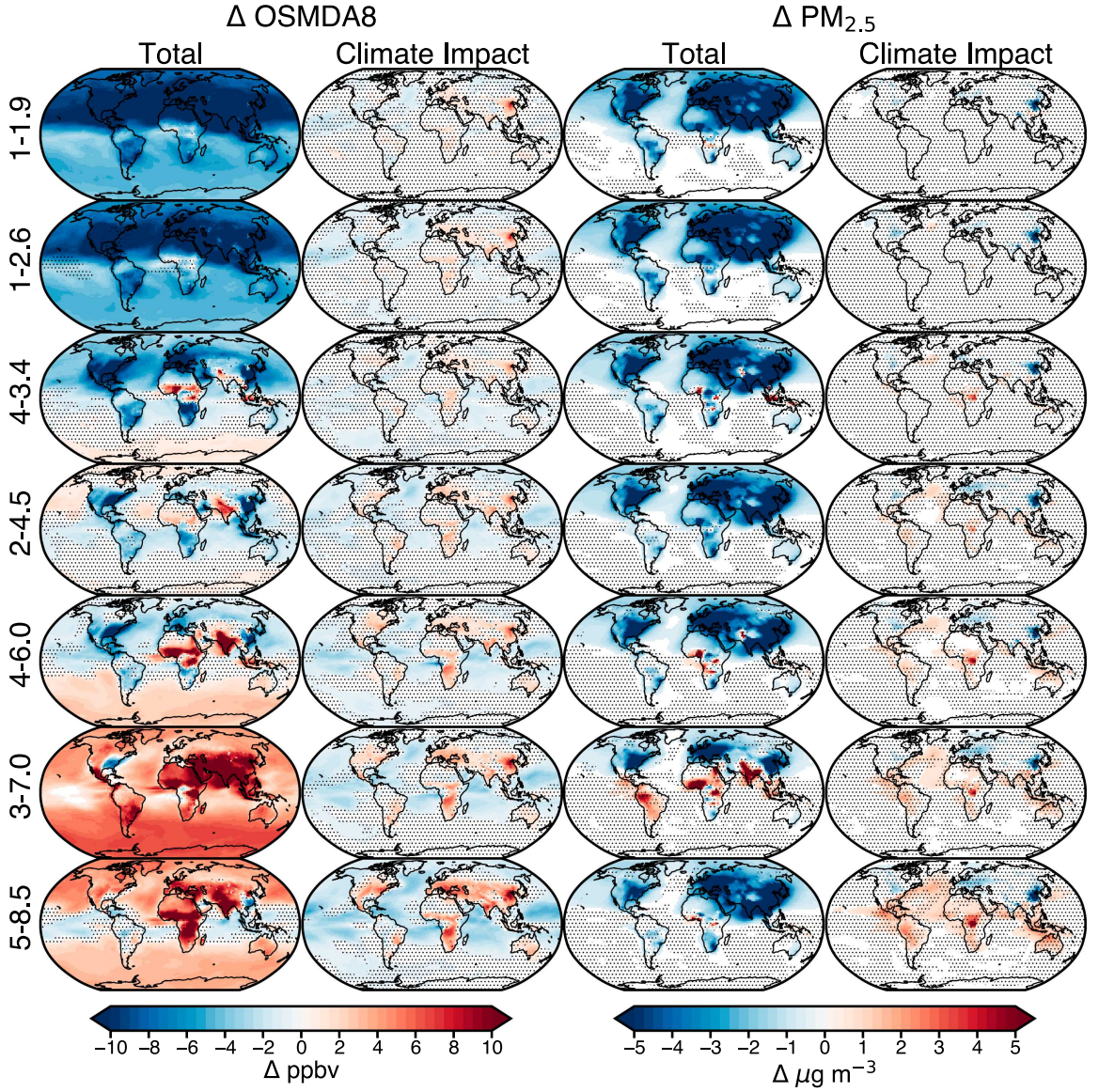


**Fig. 3.** Climate change by the end of the century will cause climate penalties to surface ozone over most land areas, as well as to nondust or non-sea-salt $PM_{2.5}$, in the Tropics and Southern Hemisphere, but climate benefits to nondust or non-sea-salt $PM_{2.5}$ over land over the Northern Extratropics. The panels show simulated future changes in 2090 to 2090 CE air quality metrics (see main text for definitions) with respect to 2005 to 2014 CE for decadal mean ozone season maximum daily 8-h average (OSMDA8) in ppbv (*Left* two columns) and decadal mean $PM_{2.5}$ in μg $m^{-3}$ (*Right* two columns). Rows from *Top* to *Bottom* show seven SSP scenarios with increasing levels of future warming. For each metric, we show the total forecasted change (columns one and three) and the change attributed to changing meteorology alone (columns two and four). Stippling indicates local changes that are statistically *insignificant* with respect to interannual variability (i.e., $P > 0.05$).

We next explain the causes of these concentration changes in the model.

Ozone in the troposphere is produced by the oxidation of CO, methane ($CH_4$), and nonmethane volatile organic compounds (NMVOCs) in the presence of reactive nitrogen oxides ($NO_x$) and sunlight. It is destroyed by sunlight in the presence of water vapor or, in heavily polluted areas, by reaction with $NO_x$. Earlier studies have found generally linear relationships between tropospheric ozone abundances and total emissions of $NO_x$ or methane (e.g., ref. 18). Fig. 1 shows the global annual emissions of ozone precursors, and *SI Appendix*, Figs. S1 and S2 show the spatial distribution of these changes. In our simulations, the total change in future surface ozone largely follows the anthropogenic emission trends. This is especially apparent in the SSP3-7.0 scenario, with its extreme increase in methane and $NO_x$ emissions with respect to the other scenarios (including the most extreme warming scenario). However, we forecast general climate penalties over land and benefits over the oceans. The benefits over the ocean reflect the exponential increase of water vapor abundances with linear increases in air temperature following the Clausius–Clapeyron relationship in regions far from precursor emissions. This is consistent with the sign of the marine ozone benefit found in the analysis of the CMIP6 CCMs (15). However, we see a more subdued change than CMIP6, likely reflecting the inclusion of tropospheric reactive halogen chemistry in our CTM that is not included in the CCMs, which reduces the relative changes in ozone over the oceans that would otherwise result from changes in terrestrial $NO_x$ and reduced carbon emissions. (e.g., refs. 19 and 20). These benefits also extend to a few land areas, such as the Gulf Coast of the southeastern United States, the Amazon rainforest, Alaska, and Siberia. However, most land regions experience ozone

penalties reflecting increases in natural ozone precursor emissions that outcompete the increased loss rate. The global natural $NO_x$ emissions are forecast to increase monotonically with increasing warming; however, we note that whether lightning will increase or decrease in the future remains highly uncertain (e.g., refs. 21–23). The increase in NMVOC emissions from terrestrial plants is not monotonic but generally increases with increased warming. These natural emission precursors and temperature-driven faster reaction rates collectively drive the surface ozone climate penalties over land. Our results are generally consistent with earlier ozone penalty studies studying comparable scenarios over the populated regions of eastern North America (15, 24–27), Europe (15, 26), and the North China Plain (15, 26), although our statistically significant penalties are more widespread. Over India, previous work has disagreed on the sign of the climate-driven change, but we agree with more recent estimates (15, 26).

$PM_{2.5}$ is composed of multiple components that are highly variable in space and time. Inorganic sulfate-nitrate-ammonium (SNA) particles primarily result from the oxidation of anthropogenic sulfur dioxide ($SO_2$) or biogenic marine dimethylsulfide (DMS) emissions, primarily within cloud droplets, with the total condensed-phase mass and speciation highly sensitive to ammonia ($NH_3$) emissions from livestock and anthropogenic and natural $NO_x$ emissions. Primary black carbon (BC; soot) and organic carbon (OC) are directly emitted by the burning of fossil and biofuels. Secondary organic aerosol (SOA) particles result from the oxidation of gas-phase NMVOCs emitted from the biosphere, producing lower-volatility species that then condense into droplets. Last, wind releases fine mineral dust and sea salt particles into the atmosphere from the land and ocean surfaces. All these $PM_{2.5}$ types then persist in the atmosphere until removal by dry or wet deposition to the surface.

Fig. 2 shows the global annual $PM_{2.5}$ direct and precursor emissions, and *SI Appendix*, Figs. S3 and S4 show the spatial distribution of these changes. In most scenarios, anthropogenic $SO_2$, BC, and OC emissions decrease in the future. However, $NH_3$ is generally assumed to increase given its tight linkage to agriculture and the need to feed a growing global population. Of the natural precursor emissions, only marine DMS and terrestrial plant NMVOCs respond to climate change in our model, and we find relatively minor increases in DMS emissions with increasing temperature. In contrast, our simulated fine mineral dust emissions have considerable interannual and spatial variability in all of our simulations, making no statistically different changes (*Lower Right* panel of Fig. 2) but dominating total changes. Meanwhile, our forecasted changes in sea-salt emissions are relatively small. Given the significant uncertainties and difficulties in simulating mineral dust emissions (e.g., ref. 28), and the availability of a global observational constraint for nondust and non-sea-salt $PM_{2.5}$ abundances (29), we interpret here only the changes in $PM_{2.5}$ due to nondust and non-sea-salt particles. Furthermore, the CMIP6 experimental design we replicate here includes all wildfires and crop burning in the prescribed anthropogenic scenarios (10). As our CTM lacks a dynamic fire module, it is not possible for us to isolate the role of climate change alone on smoke $PM_{2.5}$ here. However, we note that whether or not $PM_{2.5}$ represents a climate penalty or benefit to mortality will likely ultimately reflect climate-driven changes in fine mineral dust and smoke (e.g., refs. 30–32).

As with ozone, the total forecasted changes in $PM_{2.5}$ largely reflect changes in their direct or precursor anthropogenic emissions. However, net climate benefits to nondust and non-sea-salt $PM_{2.5}$ in the Northern Extratropics result from the forecasted increase in precipitation with increasing temperature over the heavily industrialized regions of eastern North America, Northern Europe, and East Asia. These are regions where inorganic SNA particles primarily dominate the $PM_{2.5}$ composition, and the increase in precipitation decreases the $PM_{2.5}$ lifetime and, thereby, abundances. Increased terrestrial NMVOC emissions also play a role by increasing the conversion of anthropogenic $NO_x$ to shorter-lived organic nitrates, thereby reducing total nitrate abundance. In contrast, the Tropics and Southern Hemisphere (including the United States Gulf Coast) generally forecast climate penalties resulting from increased emissions of SOA precursors from the terrestrial biosphere and faster oxidation rates.

**Impact on Mortality.** Ozone has long been known to contribute to mortality through chronic respiratory diseases (CRD). Here, we use a log–linear relationship between exposure and CRD mortality for all ages as described by Malashock et al. (33). $PM_{2.5}$ has also long been known to contribute to mortality via cardiopulmonary diseases and, in the previous decade, was definitively linked to lung cancer (LC). Here, we consider the impact of $PM_{2.5}$ on mortality using two separate exposure models used in the most recent Global Burden of Disease (GBD) report, the Meta-Regression Bayesian, Regularized, Trimmed (MR-BRT) model and the Global Exposure Mortality Model (GEMM) (1, 34, and see *Materials and Methods*). Both $PM_{2.5}$ exposure models incorporate quinquennial age-dependent exposure relationships for ischemic heart disease (IHD) and strokes, with age-independent relationships for chronic obstructive pulmonary disease (COPD), LC, type-II diabetes mellitus (DM), and lower respiratory illnesses (LRI).

*SI Appendix*, Table S1 summarizes our mortality calculations. For the recent past (2005 to 2014 CE), we calculate total mortality attributable to ambient air pollution to be 3.3 (95% CI 2.0 to 5.0) million (M) preventable deaths per year when using the MR-BRT $PM_{2.5}$ exposure model and 5.0 (3.0 to 7.4) M avoidable deaths per year when using the GEMM $PM_{2.5}$ exposure model (including dust and fine sea-salt particles), statistically consistent with the 2019 (GBD 2019) study estimate of 3.6 (2.8 to 4.4) for the same period (35). These estimates are comparable to or slightly higher than most earlier studies of the same period (2), but lower than the original GEMM analysis of 8.9 (7.5 to 10) for the year 2015 (34). The fraction of air pollution mortality attributable to fine mineral dust or sea-salt particles was 6% in the MR-BRT model and 4% in the GEMM. Global mortality attributable to ozone pollution was 350 (180 to 540) thousand (k) preventable deaths per year, consistent with those calculated for the same period for the GBD (35) as well as those determined for 2000 to 2019 CE by Malashock et al. (33). Global mortality attributable to $PM_{2.5}$ following the MR-BRT exposure model was 3.0 (1.8 to 4.4) M deaths per year, with 33% due to IHD, 32% due to stroke, 16% due to COPD, 7% due to LRI, 8% due to LC, and 4% due to DM. Mortality associated with $PM_{2.5}$ following the GEMM exposure model is 4.7 (2.8 to 6.8) M deaths per year, with 29% due to IHD, 27% due to stroke, 18% due to COPD, 13% due to LRI, 8% due to LC, and 5% due to DM.

First, we consider the impacts on mortality associated with only the forecasted climate-driven changes in air pollutants. Fig. 4 shows the climate penalties and benefits of ozone and $PM_{2.5}$ (excluding dust and sea salt) for the end of the century for the Northern Extratropics versus the Tropics and Southern Hemisphere (see *SI Appendix*, Fig. S5 for definition) if the population distribution and baseline mortality rates remained unchanged from the recent past. The climate penalty of ozone on mortality is 20 ± 1.5 k additional deaths per year per °C of further warming in the Northern Extratropics, and

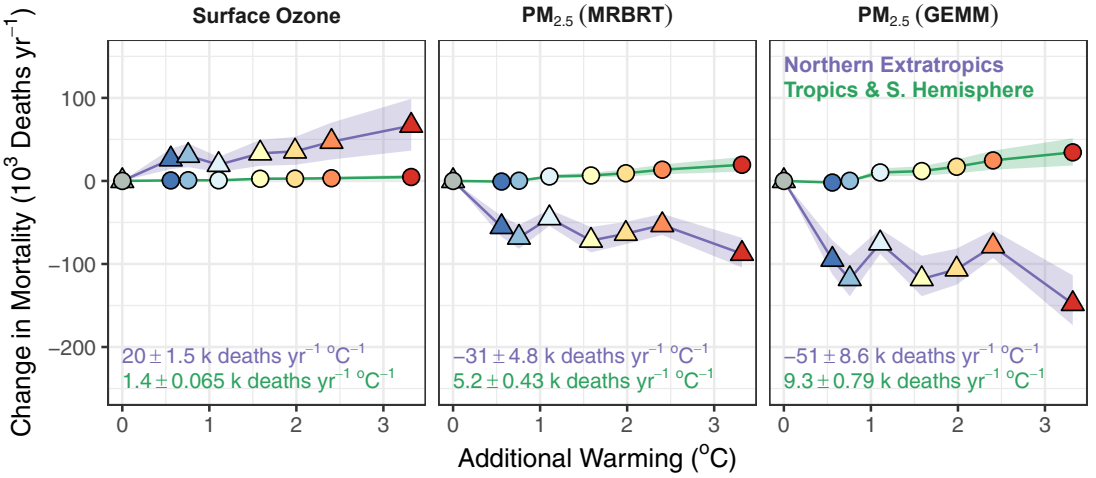


**Fig. 4.** Future climate penalties and benefits on surface air pollution depend on location. The panels present the change in annual mortality over the 2090 to 2099 CE period in thousands of avoidable deaths attributable to climate-driven changes to air pollution shown per degree Celsius of additional warming relative to 2005 to 2014 CE. These scenarios assume present-day emissions of pollution sources as well as present-day population and baseline mortality rates. The *Left* panel shows surface ozone and the *Right* two panels show $PM_{2.5}$ for two exposure-response models. The triangles and purple colors reflect the Northern Extratropics, and the circles and green colors reflect the Tropics and Southern Hemisphere. The shading represents the mean $\pm 1\sigma$ in uncertainty arising from year-to-year variability and in the exposure-response models (*Materials and Methods*). The values *Inset* give the mean $\pm 1\sigma$ of the slope of a linear regression of the different scenarios.

$1.4 \pm 0.1$ k $yr^{-1}$ $°C^{-1}$ in the Tropics and Southern Hemisphere. Our forecasted climate-driven changes in global annual mortality due to ozone for the SSP3-7.0 scenario fall within the range of estimates from a recent study using three CMIP6 CCMs, although we note some differences in the exact periods, diseases, populations, and exposure-response functions considered (36).

In the Northern Extratropics, the climate benefit of nondust and non-sea-salt $PM_{2.5}$ on mortality is $31 \pm 4.8$ k reduced deaths per °C of additional warming in the MR-BRT relative risk model, and $51 \pm 8.6$ k $yr^{-1}$ $°C^{-1}$ in the GEMM. In the Tropics and the Southern Hemisphere, the climate penalty is $5.2 \pm 0.4$ k $yr^{-1}$ $°C^{-1}$ and $9.3 \pm 0.8$ k $yr^{-1}$ $°C^{-1}$, respectively. However, the population distribution at the end of the century is forecast to be substantially different than in the recent past, with most of this century's population growth occurring in Sub-Saharan Africa and with population decreases in East Asia. If we apply the forecasted population distribution for 2095, scaled to the 2010 total population, to both our present-day and future exposure metrics, then the climate penalties for ozone on mortality become more similar between the hemispheres. However, the Northern Extratropical climate benefit of $PM_{2.5}$ to mortality increases by about 75% in either exposure model, and the Tropics and Southern Hemisphere climate penalty of $PM_{2.5}$ to mortality increases by about 300% (*SI Appendix*, Fig. S6). Last, we note that uncertainty in the future localized climate impact of $PM_{2.5}$ over India (*SI Appendix*, Figs. S7 and S8) contributes substantial noise on top of the overall trend (Fig. 4; India is classified Northern Extratropics here), and we likely need additional ensembles members to reduce the uncertainty in this very populous and vulnerable region.

**Impact on Global Food Security.** Ozone is a biological irritant and has long been known to damage vegetation and crops, resulting in tens of millions of metric tons of crop production losses with economic impacts in the tens of billions of dollars in the recent past (e.g., refs. 4 and 37). We test three different empirically derived exposure-crop yield models for five major cash crops (*Materials and Methods*) and estimate global crop losses in the recent past (2005 to 2014 CE) of 4.4 to 20% for winter wheat, 0.4 to 7.6% for spring wheat, 1.1 to 7.3% for soybeans, 0.7 to 4.3% for rice, and 0.2 to 2.9% for maïze, resulting in economic losses of $10 to 63 billion in 2010 United States Dollars ($USD_{2010}$). These are consistent with earlier estimates of losses in the recent past, although uncertainties remain large (e.g., refs. 4 and 37).

Fig. 5 shows the change in crop production in million metric tons (Mmt) per year as a function of additional warming in 2090 to 2099 CE relative to 2005 to 2014 CE due to climate change alone. The total change (including anthropogenic emissions and

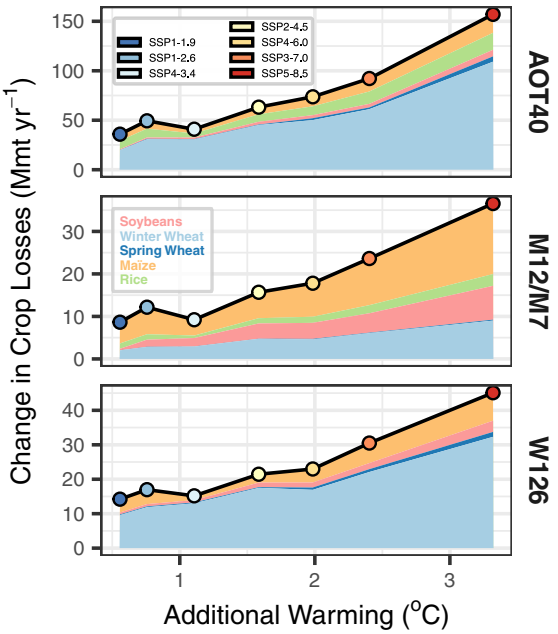


**Fig. 5.** Forecasted changes in crop losses due to surface ozone change at the end of the century (2090 to 2095 CE) relative to the recent past (2005 to 2014 CE) associated with climate change alone as a function of additional changes in global mean surface air temperature relative to 2005 to 2014 CE, for three different crop-exposure metrics (rows). The total is shown as the black line, with the individual contributions to each major cash crop shown as shaded ribbons for soybeans (pink), winter wheat (light blue), spring wheat (dark blue), maïze (orange), and rice (light green).

climate change) largely follows the anthropogenic emissions, especially methane (*SI Appendix*, Fig. S9). We find increased food production due to ozone changes alone in the most extreme mitigation scenarios but decreases in food production in the most extreme warming scenarios, particularly due to ozone-sensitive winter wheat. The inflection point year from decreased to increased losses differs per metric, but all scenarios that meet the Paris Agreement find net savings in crop production. However, these savings are still offset by the climate-driven increase in surface ozone over land. We calculate climate penalties of 22 ± 6.8 Mmt $yr^{-1}$ $°C^{-1}$, resulting in economic losses of \$6.7 ± 2.0 billion $USD_{2010}$ $yr^{-1}$ $°C^{-1}$.

**Conclusions.** Climate change alone will lead to changes in surface air pollution. Here, we applied a CTM driven by meteorology archived from a climate model for the end of this century relative to the recent past in order to isolate the impact of changing meteorology versus anthropogenic emissions on surface ozone and $PM_{2.5}$. Surface ozone generally increases over land with warming temperatures because of increases in natural precursor emissions. $PM_{2.5}$ in the Northern Extratropics generally decreases due to increased loss processes but increases in the Tropics and Southern Hemisphere due to increased organic precursor emissions from the terrestrial biosphere. Collectively, this leads to a net climate benefit from all air pollution on mortality. However, the benefits are localized to the most industrialized regions of the world, with net penalties in regions of the world expected to contain the most coming population growth. Globally, we find net climate penalties everywhere on crop production.

Nevertheless, these results contain large uncertainties. For mortality, the large uncertainty in the epidemiological exposure-response relationships (2) dominates over internal variability of the atmosphere (i.e., interannual variability in pollution exposure); it is important that future epidemiological studies reduce these uncertainties. The internal variability is not insignificant, especially for the more subdued warming scenarios (Fig. 3), and future studies should try to incorporate additional ensemble members per decade and climate scenario to improve the signal-to-noise of the climate impacts, with especial focus on South Asia. And as we note, emissions of fine mineral dust and smoke $PM_{2.5}$, which we had to exclude from our analysis, remain highly uncertain but will likely dominate future climate-driven $PM_{2.5}$ changes, so we recommend further analyses dedicated to improving representation of these sources in CTMs. There are also known imperfections with the exposure-based metrics used in this study for crop yields, so it would be beneficial for CTMs to implement online crop diagnostics using flux-based methods (e.g., ref. 4).

Last, we note that the overall change in both pollutants is dominated by the anthropogenic emission trajectory, whereas the global climate response is primarily dominated by the atmospheric $CO_2$ abundance. Yet the most extreme warming scenario is not the most extreme air pollution precursor emission scenario in the SSPs. Therefore, we recommend studies aimed at predicting future air quality take into consideration a wider range of possible air pollution precursor trajectories and that we include CTMs whenever possible in future climate change assessment reports.

## Materials and Methods

**Simulations.** We use version 2 of the Global Change and Air Pollution (GCAP2) model framework, which is described in detail by Murray et al. (17). In brief, simulations of the NASA Goddard Institute for Space Studies ModelE2.1 general circulation model (38) performed for CMIP6 were rerun to archive meteorological input files necessary to drive version 13.4.1 of the GEOS-Chem global 3-D CTM (with a correction applied to a bug in the code meant to guarantee mass conservation during transport). These ModelE2.1 simulations relied on atmospheric composition taken from earlier transient simulations that included tropospheric chemistry and, therefore, captured the first-order chemistry-climate feedback of the parent CCM on the meteorology. This includes the influence of future ozone changes on stratospheric dynamics. Tropospheric chemistry will therefore respond to changes in stratosphere-to-troposphere exchange, as well as changes in overhead ozone columns, which will affect photolysis rates. Anthropogenic emissions (which include biomass burning) are as defined by the CMIP6 experiment for the recent past and seven future emission scenarios (9, 10). Lightning $NO_x$ production in the model responds positively to increases in convective cloud-top height, and the parent CCM and coupled GCM-CTM share a consistent treatment of lightning flash generation and $NO_x$ distribution (17, 39). $NO_x$ from soil microbial activity responds positively with surface temperature, cloud fraction, and wind speed, negatively with radiation and snow/ice cover, and variably with soil wetness (40). Biogenic emissions of NMVOCs from terrestrial plants respond positively to increases in diffuse shortwave radiation, surface temperature, and soil wetness (41), and we do not consider the possible role of $CO_2$ inhibition (e.g., ref. 4) in these simulations. Biogenic emissions of marine NMVOCs and DMS respond positively to sea-surface temperatures and surface wind speeds (42). Natural emissions of $SO_2$ from volcanoes and $NH_3$ from wild animals are assumed to be invariant in time.

We first perform a baseline simulation for 2005 to 2014 CE. For each of the seven future climate scenarios, we then perform three simulations: one in which anthropogenic emissions are prescribed from 2005 to 2014 CE, but the meteorology is from 2090 to 2099 CE ("climate impact"), one in which anthropogenic emissions are from 2090 to 2099 CE but the meteorology is from 2005 to 2014 CE ("emissions impact"), and one in which both the emissions and meteorology are from 2090 to 2099 CE ("both impacts"). The "climate impact" simulations include changes in natural emissions that are sensitive to meteorology. As is common in global atmospheric chemistry models, methane is prescribed as a surface boundary condition in GEOS-Chem. We include the impact of future methane abundance as a chemical reactant in the "emissions impact" simulation, while the "climate impact" simulation includes radiative-driven impacts of methane abundances on meteorology (e.g., temperature, water vapor abundance). All wildfires are prescribed in the anthropogenic emissions, per the CMIP6 experimental design (10). We assess the linearity of the system in *SI Appendix*, Figs. S10 and S11 and find the sum of the estimated emissions and climate impacts alone to largely match the total changes.

Each simulation was initialized over 15 y at a degraded horizontal resolution of 4° latitude by 5° longitude. Then each simulation was performed for ten years at the full model resolution of 2° latitude by 2.5° longitude with 40 vertical layers extending from the surface to 0.1 hPa. Hourly surface ozone and monthly mean $PM_{2.5}$ were archived and regridded using a first-order conservative remapping algorithm (43) to 0.5° horizontal resolution for calculating the mortality and crop impacts. $PM_{2.5}$ at 35% relative humidity is a standard diagnostic output of GEOS-Chem, with speciation available for inorganic sulfate-nitrate-ammonium, black carbon, mineral dust, sea salt, and primary and secondary organic particles at and under 2.5 μm in diameter.

**Mortality Calculation.** For mortality due to surface ozone, we use the ozone season maximum daily 8-h average (OSMDA8) exposure metric, which is calculated as the 10-y average annual maximum of the 6-mo running mean of the monthly average daily maximum 8-h mixing ratio in ppbv (1 ppbv ≡ 1 nmol $mol^{-1}$). For mortality due to $PM_{2.5}$, the exposure metric is the simple 10-y climatological mean surface concentration. In both cases, we remove each metric's local 2005 to 2014 CE climatological mean bias with respect to observational constraints. For OSMDA8, this is the 2005 to 2014 CE climatological mean reanalysis value of DeLang et al. (44), and for $PM_{2.5}$, this is the 2005 to 2014 CE climatological mean value from version V4.GL.03 of the Hammer et al. hybrid satellite-model product (29). In both cases, we assume the bias to be invariant in time. For all mortality calculations, we use the historical Hammer et al. sea-salt and dust $PM_{2.5}$ product in lieu of the simulated values (see main text for explanation), and therefore our calculated mortality changes do not include either of these $PM_{2.5}$ species.

Mortality attributed to a specific cause ($\Delta M$) at a given location is calculated as

$$\Delta M = y_c \cdot AF \cdot P, \quad [1]$$

where $y_c$ is the baseline subnational (United States, Brazil, and Indonesia) or national (all other countries) age-specific mortality rate in 2010 for cause of death $c$ from the 2019 GBD study (*SI Appendix*, Fig. S12; ref. 35), $AF$ is the attribution function that relates the changes in OSMDA8 or $PM_{2.5}$ to changes in mortality, and $P$ is the local exposed relevant age-specific population for 2010 from version 4.11 of the Gridded Population of the World dataset (*SI Appendix*, Fig. S13; ref. 45). For the future population distribution, we use the age-specific 2022 Revision of World Population Prospects for the year 2095 CE developed by the United Nations (UN), accessed on 21 Feb 2023 from https://population.un.org/wpp/. The attributable fraction is calculated as

$$AF = 1 - \left(\frac{1}{RR}\right), \quad [2]$$

where $RR$ is the reported relative risk of mortality for a disease resulting from pollutant exposure, as next described.

For ozone $RR$, we use an updated version of the GBD 2019 methodology, as described by Malashock et al. (33). This assumes a log–linear relationship between $RR$ and concentration,

$$RR = \exp\left[\beta\left(X_g - X_0\right)\right], \quad [3]$$

where $\beta = 1.06$ per 10 ppbv ozone (95% CI 1.03 to 1.10) is the concentration–response factor for CRD assessed by GBD 2019 for all ages, $X_g$ is the simulated bias-corrected local decadal OSMDA8 metric, and $X_0 = 32.4$ ppbv is the theoretical minimum risk exposure level (TMREL).

For $PM_{2.5}$, we consider two different exposure models. The first is the Meta-Regression Bayesian, Regularized, Trimmed (MR-BRT) relationship between exposure and mortality developed for the GBD (1) and the second is the Global Exposure Mortality Model (GEMM; 34). Both models include quinquennial age-dependent exposure relationships for IHD and strokes at and over the age of 25, with age-independent relationships for COPD, LC, and type II DM ($P$ ages $\geq 25$) and LRI ($P$ ages $< 5$ and $\geq 25$). We use the MR-BRT and GEMM splines for $RR$ as a function of disease and $PM_{2.5}$ exposure provided by McDuffie et al., which include CIs that account for uncertainty in TMRELs (*SI Appendix*, Figs. S14 and S15; 46). In addition, we adjust the MR-BRT attributable deaths by the scale factors reported by McDuffie et al. (*SI Appendix*, Fig. S16; 46) that take into account coexposure to indoor pollution, as the MR-BRT $RR$s were developed from a meta-analysis that included indoor exposure.

To calculate the change in mortality, we calculate total attributable mortality in the recent past and each future climate simulation separately, and then take the difference. In all calculations, we use the provided $RR$ 95% CIs to estimate upper and lower limits.

**Crop Loss Calculation.** We consider the impact of ozone pollution on five staple cash crops for which concentration-based exposure metrics are available (winter wheat, spring wheat, maïze, soybeans, and rice). We examine three separate relationships defined as

$$\text{AOT40} = \sum_{i=1}^{n} \left([O_3]_i - 0.04\right) \text{ for } [O_3] \geq 0.04 \quad [4]$$

$$\text{M12} = \frac{1}{n}\sum_{i=1}^{n}\left(10^3 [O_3]_i\right) \quad [5]$$

$$\text{W126} = \sum_{i=1}^{n}\left(\frac{[O_3]_i}{1 + 4403e^{-126[O_3]_i}}\right), \quad [6]$$

where $[O_3]_i$ is the hourly mean ozone mixing ratio in ppmv (1 ppmv $\equiv$ 1 $\mu$mol mol$^{-1}$) at hour $i$, and $n$ is the number of daylight hours (8:00 to 19:59 LT) during the three-month growing season prior to harvest. The M7 metric is defined the same as M12 but uses a shorter daylight window (9:00 to 15:59 LT). AOT40 and W126 have units of ppmv h, and M12 and M7 have units of ppbv. Tai et al. (4) argued that the three concentration-based metrics vary enough for individual crops that they likely cover the full uncertainty space; improved flux-based and biophysical estimates (not presently implemented within the CTM) likely fall within these uncertainty ranges.

We remove the local daily climatological daytime (6:00 to 17:59 LT) mean bias of surface ozone from our simulations to generate the most accurate baseline calculation and because the exposure-relative yield calculations are nonlinear with respect to concentration. First, we aggregate hourly daytime surface ozone mixing ratios from 2005 to 2014 CE for the United States, Canada, Mexico, Europe, and the Global Atmospheric Watch program, as well as more recent data available for China and India, totaling over 290 million observations (see *SI Appendix*, Table S2 for data sources). We then trained a random-forest regression model (e.g., ref. 47) using 10-fold cross-validation to predict the bias for unobserved locations as a function of relevant simulated meteorological, emission, geographic, and temporal factors, as well as population density (see *SI Appendix*, Table S3 for parameters). We used a randomly selected 80% of the observations and their 2005 to 2014 CE simulated counterparts for training and the remaining 20% for evaluation ($RMSE = 2.9$ ppbv; *SI Appendix*, Fig. S17). We assumed the present-day climatological bias to be invariant across the 21st century and removed the local daily mean bias from all our simulations before calculating each metric for each future scenario.

We assume the growing season for each crop to be the local mean day of the year of each crop harvest from the Crop Calendar Dataset (*SI Appendix*, Fig. S18; 48) and 89 d prior. We evaluate the ability of the bias-corrected model

**Table 1. Crop relative yield (*RY*) with respect to a yield with no loss due to ozone as a function of exposure metric *x***

| | | Winter wheat | | Spring wheat | | Rice | | Soybeans | | Maïze | | Region | |
|---|---|---|---|---|---|---|---|---|---|---|---|---|---|
| $x$ | $RY$ | $a$ | $b$ | $a$ | $b$ | $a$ | $b$ | $a$ | $b$ | $a$ | $b$ | applied | Refs. |
| AOT40 | $\frac{1-a^{x+1.08(40-b)-(20.22-0.01264b^2)}}{1-a^{(22.98-1.08b+0.01264b^2)}}$ | 0.0161 | 26.5 | 0.0161 | 26.5 | 0.0071 | 19.4 | | | 0.0068 | 40 | E. Asia* | (5) |
| | $1 - ax$ | | | | | | | 0.012 | | | | China | (51) |
| | $0.98 - ax$ | 0.039 | | 0.019 | | | | | | | | S. Asia† | (52) |
| | $0.98 - ax$ | 0.024 | | 0.024 | | | | | | | | Europe‡ | (53) |
| | $1.01 - ax$ | 0.014 | | 0.014 | | | | | | | | N. America | (53) |
| | $1 - ax$ | 0.0163 | | 0.0163 | | 0.00415 | | 0.0113 | | 0.00356 | | ROTW | (54) |
| M7 | $e^{-\left(\frac{x}{a}\right)^b}/e^{-\left(\frac{25}{a}\right)^b}$ | 137 | 2.34 | 186 | 3.20 | 202 | 2.47 | | | | | World | (54) |
| M12 | $e^{-\left(\frac{x}{a}\right)^b}/e^{-\left(\frac{20}{a}\right)^b}$ | | | | | | | 107 | 1.58 | 124 | 2.83 | World | (54) |
| W126 | $1 - ax$ | | | | | | | 0.0074 | | | | China | (51) |
| | $e^{-\left(\frac{x}{a}\right)^b}$ | 51.2 | 1.747 | 51.2 | 1.747 | | | 109.75 | 1.2315 | 93.7 | 3.392 | ROTW | (55) |

*China, Japan, and Korea; †Mainland Asia, excluding China, Japan, Korea, and Russia; ‡Includes Russia.

to accurately estimate variability in the exposure metrics calculated directly from the observations and find excellent agreement with all $R^2 > 0.9$ (*SI Appendix*, Fig. S19).

Each crop's relative yield (*RY*) with respect to no ozone is determined via the exposure-relative yield relationships with each respective metric as described in Table 1. The relative yield loss (*RYL*) is, therefore, $1 - RY$, and crop production loss (*CPL*) is, therefore, $\frac{CP}{RY} RYL$, where *CP* is the local crop production data (including losses) in metric tons per square kilometer from the Spatial Production Allocation Model for 2010 (SPAM2010; *SI Appendix*, Fig. S20; 49). We split the total wheat production reported by SPAM2010 between its spring and winter varietals using those ratios from the Group on Earth Observations Global Agricultural Monitoring Best Available Crop Specific (GEOGLAM-BACS) masks (50) since the M7 metric shows higher sensitivity of winter wheat to ozone. Some tropical countries have two or three harvest seasons for rice or maïze; in these cases, we attribute all production to the primary growing season, as has been done in earlier studies (e.g., ref. 4).

Crop production losses are then converted into economic losses using national prices per crop for 2010 in United States Dollars ($USD_{2010}$) from the UN Food and Agriculture Organization Corporate Statistical Database (FAOSTAT; accessed 15 Sep 2022). Locations in countries that did not report to FAOSTAT in 2010 are filled in using the value of their nearest neighbor (*SI Appendix*, Fig. S21).

**Data, Materials, and Software Availability.** Gridded model output and data products necessary for performing the mortality and crop yield impacts have been deposited to Zenodo (56). Access to the GCAP2 source code and data input are as described in Murray et al. (17). All other data are included in the manuscript and/or *SI Appendix*.

**ACKNOWLEDGMENTS.** This research has been supported by the NSF (grant nos. AGS-1702106 and AGS-2002414 to L.T.M.) for model development and the University of Rochester for simulation and analysis. We thank Jason West (University of North Carolina at Chapel Hill) for providing the annual gridded ozone product from DeLang et al., and Erin McDuffie and Marcus Sarofim (United States Environmental Protection Agency) for providing useful feedback.

Author affiliations: [a]Department of Earth and Environmental Sciences, University of Rochester, Rochester, NY 14627; [b]Department of Physics and Astronomy, University of Rochester, Rochester, NY 14627; [c]Department of Physics and Astronomy, Ithaca College, Ithaca, NY 14850; [d]John A. Paulson School of Engineering and Applied Sciences, Harvard University, Cambridge, MA 02138; [e]Department of Earth and Environmental Sciences, The Chinese University of Hong Kong, Hong Kong Special Administrative Region 852, China; [f]State Key Laboratory of Agrobiotechnology, The Chinese University of Hong Kong, Hong Kong Special Administrative Region 852, China; and [g]Institute of Environment, Energy and Sustainability, The Chinese University of Hong Kong, Hong Kong Special Administrative Region 852, China

1. GBD, 2019 Risk Factors Collaborators, Global burden of 87 risk factors in 204 countries and territories, 1990-2019: A systematic analysis for the Global Burden of Disease Study 2019. *Lancet* **396**, 1223–1249 (2020).
2. A. Pozzer *et al*., Mortality attributable to ambient air pollution: A review of global estimates. *Geohealth* **7**, e2022GH000711 (2023).
3. L. Emberson, Effects of ozone on agriculture, forests and grasslands. *Philos. Trans. A Math. Phys. Eng. Sci.* **378**, 20190327 (2020).
4. A. P. K. Tai, M. Sadiq, J. Y. S. Pang, D. H. Y. Yung, Z. Feng, Impacts of surface ozone pollution on global crop yields: Comparing different ozone exposure metrics and incorporating co-effects of $CO_2$. *Front. Sustain. Food Syst.* **5**, 2021 (2021).
5. Z. Feng *et al*., Ozone pollution threatens the production of major staple crops in East Asia. *Nat. Food* **3**, 47–56 (2022).
6. D. J. Jacob, D. A. Winner, Effect of climate change on air quality. *Atmos. Environ.* **43**, 51–63 (2009).
7. A. P. K. Tai, M. V. Martin, C. L. Heald, Threat to future global food security from climate change and ozone air pollution. *Nat. Clim. Chang.* **4**, 817–821 (2014).
8. A. Fiore, V. Naik, E. Leibensperger, Air quality and climate connections. *J. Air Waste Manag. Assoc.* **65**, 645–685 (2015).
9. R. M. Hoesly *et al*., Historical (1750–2014) anthropogenic emissions of reactive gases and aerosols from the Community Emissions Data System (CEDS). *Geosci. Model. Dev.* **11**, 369–408 (2018).
10. M. J. Gidden *et al*., Global emissions pathways under different socioeconomic scenarios for use in CMIP6: A dataset of harmonized emissions trajectories through the end of the century. *Geosci. Model. Dev.* **12**, 1443–1475 (2019).
11. M. J. E. van Marle *et al*., Historic global biomass burning emissions for CMIP6 (BB4CMIP) based on merging satellite observations with proxies and fire models (1750–2015). *Geosci. Model. Dev.* **10**, 3329–3357 (2017).
12. S. Wu, L. J. Mickley, D. J. Jacob, D. Rind, D. G. Streets, Effects of 2000–2050 changes in climate and emissions on global tropospheric ozone and the policy-relevant background surface ozone in the United States. *J. Geophys. Res.* **113**, D18312 (2008).
13. T. M. Fu, H. Tian, Climate change penalty to ozone air quality: Review of current understandings and knowledge gaps. *Curr. Pollut. Rep.* **5**, 159–171 (2019).
14. A. P. K. Tai, L. J. Mickley, D. J. Jacob, Impact of 2000–2050 climate change on fine particulate matter ($PM_{2.5}$) air quality inferred from a multi-model analysis of meteorological modes. Atmospheric. *Chem. Phys.* **12**, 11329–11337 (2012).
15. P. Zanis *et al*., Climate change penalty and benefit on surface ozone: A global perspective based on CMIP6 earth system models. *Environ. Res. Lett.* **17**, 024014 (2022).
16. T. Glotfelty, Y. Zhang, P. Karamchandani, D. G. Streets, Changes in future air quality, deposition, and aerosol-cloud interactions under future climate and emission scenarios. *Atmos. Environ.* **139**, 176–191 (2016).
17. L. T. Murray, E. M. Leibensperger, C. Orbe, L. J. Mickley, M. Sulprizio, GCAP 2.0: A global 3-D chemical-transport model framework for past, present, and future climate scenarios. *Geosci. Model. Dev.* **14**, 5789–5823 (2021).
18. P. J. Young *et al*., Pre-industrial to end 21st century projections of tropospheric ozone from the Atmospheric Chemistry and Climate Model Intercomparison Project (ACCMIP). *Atmos. Chem. Phys.* **13**, 2063–2090 (2013).
19. J. P. Parrella *et al*., Tropospheric bromine chemistry: Implications for present and pre-industrial ozone and mercury. *Atmos. Chem. Phys.* **12**, 6723–6740 (2012).
20. X. Wang *et al*., The role of chlorine in global tropospheric chemistry. *Atmos. Chem. Phys.* **19**, 3981–4003 (2019).
21. L. T. Murray, Lightning $NO_x$ and impacts on air quality. *Curr. Pollut. Rep.* **2**, 115–133 (2016).
22. C. G. Price, Lightning applications in weather and climate research. *Surv. Geophys.* **34**, 755–767 (2013).
23. E. Williams, Lightning and climate: A review. *Atmos. Res.* **76**, 272–287 (2005).
24. H. E. Rieder, A. M. Fiore, L. W. Horowitz, V. Naik, Projecting policy-relevant metrics for high summertime ozone pollution events over the eastern united states due to climate and emission changes during the 21st century. *J. Geophys. Res. Atmos.* **120**, 784–800 (2015).
25. H. E. Rieder *et al*., Combining model projections with site-level observations to estimate changes in distributions and seasonality of ozone in surface air over the U.S.A. *Atmos. Environ.* **193**, 302–315 (2018).
26. J. Schnell *et al*., Effect of climate change on surface ozone over North America, Europe, and East Asia. *Geophys. Res. Lett.* **43**, 3509–3518 (2016).
27. C. Nolte *et al*., Regional temperature-ozone relationships across the U.S. under multiple climate and emissions scenarios. *J. Air Waste Manag. Assoc.* **71**, 1251–1264 (2021).
28. A. Zhao, C. L. Ryder, L. J. Wilcox, How well do the CMIP6 models simulate dust aerosols. *Atmos. Chem. Phys.* **22**, 2095–2119 (2022).
29. M. Hammer *et al*., Global estimates and long-term trends of fine particulate matter concentrations (1998–2018). *Environ. Sci. Technol.* **54**, 7879–7890 (2020).
30. X. Yue, L. Mickley, J. Logan, J. Kaplan, Ensemble projections of wildfire activity and carbonaceous aerosol concentrations over the western United States in the mid-21st century. *Atmos. Environ.* **1994**, 767–780 (2013).
31. B. Ford *et al*., Future fire impacts on smoke concentrations, visibility, and health in the contiguous United States. *Geohealth* **2**, 229–247 (2018).
32. P. Achakulwisut *et al*., Effects of increasing aridity on ambient dust and public health in the U.S. Southwest under climate change. *Geohealth* **3**, 127–144 (2019).
33. D. Malashock *et al*., Global trends in ozone concentration and attributable mortality for urban, peri-urban, and rural areas between 2000 and 2019: A modelling study. *Lancet Planet. Health* **6**, e958–e967 (2022).
34. R. Burnett *et al*., Global estimates of mortality associated with long-term exposure to outdoor fine particulate matter. *Proc. Natl. Acad. Sci. U.S.A.* **115**, 9592–9597 (2018).
35. Global Burden of Disease Collaborative Network, Data from "Global Burden of Disease Study 2019 Results." GHDx. https://ghdx.healthdata.org/gbd-2019. Accessed 17 August 2023.
36. D. Akritidis *et al*., Strong increase in mortality attributable to ozone pollution under a climate change and demographic scenario. *Environ. Res. Lett.* **19**, 024041 (2024).
37. S. Avnery, D. L. Mauzerall, J. Liu, L. W. Horowitz, Global crop yield reductions due to surface ozone exposure: 1. Year 2000 crop production losses and economic damage. *Atmos. Environ.* **45**, 2284–2296 (2011).
38. L. S. Nazarenko *et al*., Future climate change under SSP emission scenarios with GISS-E2.1. *J. Adv. Model. Earth Syst.* **14**, e2021MS002871 (2022).
39. M. Kelley *et al*., GISS-E2.1: Configurations and climatology. *J. Adv. Model. Earth Syst.* **12**, e2019MS002025 (2020).
40. R. C. Hudman *et al*., Steps towards a mechanistic model of global soil nitric oxide emissions: Implementation and space based-constraints. *Atmos. Chem. Phys.* **12**, 7779–7795 (2012).
41. A. B. Guenther *et al*., The model of emissions of gases and aerosols from nature version 2.1 (MEGAN2.1): An extended and updated framework for modeling biogenic emissions. *Geosci. Model. Dev.* **5**, 1471–1492 (2012).
42. E. Fischer, D. Jacob, D. Millet, R. Yantosca, J. Mao, The role of the ocean in the global atmospheric budget of acetone. *Geophys. Res. Lett.* **39**, L01807 (2012).
43. P. W. Jones, First- and second-order conservative remapping schemes for grids in spherical coordinates. *Mon. Weather Rev.* **127**, 2204–2204 (1999).
44. M. DeLang *et al*., Mapping yearly fine resolution global surface ozone through the Bayesian maximum entropy data fusion of observations and model output for 1990–2017. *Environ. Sci. Technol.* **55**, 4389–4398 (2021).
45. Center for International Earth Science Information Network (CIESIN), Columbia University, Data from "Gridded Population of the World, Version 4 (GPWv4): Population Count, Revision 11." SEDAC. https://doi.org/10.7927/H45Q4T5F. Deposited 28 November 2018.
46. E. McDuffie *et al*., Source sector and fuel contributions to ambient $PM_{2.5}$ and attributable mortality across multiple spatial scales. *Nat. Commun.* **12**, 3594 (2021).
47. M. Schonlau, R. Y. Zou, The random forest algorithm for statistical learning. *Stata J. Promot. Commun. Stat. Stata* **20**, 3–29 (2020).
48. W. J. Sacks, D. Deryng, J. A. Foley, N. Ramankutty, Crop planting dates: An analysis of global patterns. *Glob. Ecol. Biogeogr.* **19**, 607–620 (2010).

49. Q. Yu *et al*., A cultivated planet in 2010 - part 2: The global gridded agricultural-production maps. *Earth Syst. Sci. Data* **12**, 3545–3572 (2020).
50. I. Becker-Reshef *et al*., Crop type maps for operational global agricultural monitoring. *Sci. Data* **10**, 172 (2023).
51. W. Zhang, Z. Feng, X. Wang, X. Liu, E. Hu, Quantification of ozone exposure- and stomatal uptake-yield response relationships for soybean in Northeast China. *Sci. Total. Environ.* **599–600**, 710–720 (2017).
52. H. Pleijel, M. Broberg, J. Uddling, K. Kobayashi, Letter to the editor regarding Pleijel et al. 2019: Ozone sensitivity of wheat in different continents - an addendum. *Sci Total. Environ.* **773**, 146335 (2021).
53. H. Pleijel, M. Broberg, J. Uddling, Ozone impact on wheat in Europe, Asia and North America - a comparison. *Sci. Total. Environ.* **664**, 908–914 (2019).
54. R. Van Dingenen *et al*., The global impact of ozone on agricultural crop yields under current and future air quality legislation. *Atmos. Environ.* **43**, 604–618 (2009).
55. X. Wang, D. L. Mauzerall, Characterizing distributions of surface ozone and its impact on grain production in China, Japan and South Korea: 1990 and 2020. *Atmos. Environ.* **38**, 4383–4402 (2004).
56. L. Murray *et al.*, Estimating future climate change impacts on human mortality and crop yields via air pollution: supplemental files. Zenodo. https://doi.org/10.5281/zenodo.13363449. Deposited 22 August 2024.